THERMOACOUSTIC ANALYSIS OF DISPLACER GAP LOSS IN A LOW TEMPERATURE STIRLING COOLER

Vincent Kotsubo[1] and Gregory Swift[2]

[1]Ball Aerospace and Technologies
Boulder, CO 80027 USA

[2]Condensed Matter and Thermal Physics Group
Los Alamos National Laboratory
Los Alamos NM 87545 USA

ABSTRACT

Thermoacoustic theory is applied to oscillating flow in a parallel-plate gap with finite and unequal heat capacities on the two bounding walls, and with relative movement of one wall with respect to the other. The motivation is to understand the behavior of displacer gap losses at low temperatures in a Stirling cooler. Equations for the oscillating temperature and enthalpy flux down the gap and down the moving solid as a function of pressure amplitude, flow, temperatures, wall velocity, and material properties are derived. General expressions, along with results illustrating the behavior of the solutions, are presented. The primary result is that losses may increase significantly below 25 K, due to vanishing wall heat capacities and reduced thermal penetration depth in the helium gas.

KEYWORDS: Thermoacoustics, Stirling, Cryocooler, Displacer
PACS: 43.35.Ud

INTRODUCTION

In a Stirling cryocooler, there are two losses in the gap between the displacer and the displacer cylinder wall. One is shuttle loss, which arises from relative motion between the displacer and the wall, and the other is enthalpy flow loss due to oscillatory flow in the gap. These losses have previously been analyzed in detail, and in fact, for oscillatory flow between two stationary parallel surfaces with identical properties, software codes such as DeltaE [1], Sage [2], and REGEN3 [3] can provide solutions.

These codes, however, are deficient when applied to low temperature displacer gaps. Here, the viscous and thermal penetration depths in helium gas may become approximately equal the displacer gap, in which case REGEN3 does not apply since it uses steady flow heat transfer coefficients. Sage, which does include high frequency heat

transfer, has undemonstrated accuracy in the crossover region where the penetration depths are on the order of the gap. In addition, while all three codes have the capability to analyze the case where diminishing wall heat capacities become small compared to gas heat capacities, none of the three codes handles the case where the two bounding walls are different, as is typical of Stirling coolers, or the case where one wall may be moving and made of metal such as stainless steel or titanium, and the other may be stationary and either polymeric or a composite such as G-10.

This paper applies thermoacoustic formalism, as described in Reference 4, to such cases.

THERMOACOUSTIC THEORY

The geometry of interest is shown in FIGURE 1. The oscillatory flow is in the *x* direction, and *y* is transverse to the flow. The gas region is bounded by $\pm y_0$, and the solids have thicknesses L_S where *S* stands for *M* for a 1-layer moving solid, *Ma* and *Mb* for a 2-layer moving solid, *I* for a one-layer immobile solid, and *Ia* and *Ib* for a 2-layer immobile solid. Thus, the analysis includes many combinations of wall layering; for example, where a metallic wall is lined with a polymer that acts as a bearing surface.

In the thermoacoustic formalism, the temperature and pressure of the gas are expressed as

$$T(x,y,t) = T_m(x) + \mathrm{Re}\left[T_1(x,y)\, e^{i\omega t}\right], \tag{1}$$

$$p(x,t) = p_m + \mathrm{Re}\left[p_1 e^{i\omega t}\right], \tag{2}$$

where the subscript *m* represents mean values and the subscript 1 refers to the 1st order complex amplitude of the oscillatory part. The angular frequency of oscillation is ω.

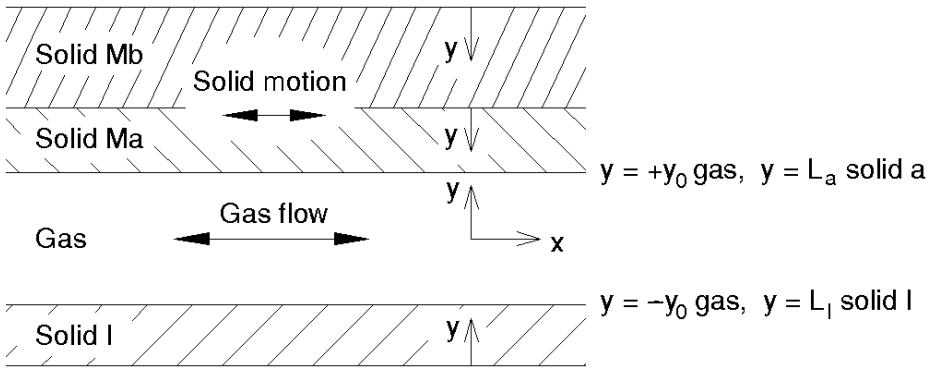

FIGURE 1. Schematic of the solution region.

The gas velocity, gas volume flow rate, and solid velocity are

$$u(x,y,t) = \mathrm{Re}\left[u_1(x,y)\, e^{i\omega t}\right], \tag{3}$$

$$U(x,t) = \mathrm{Re}\left[U_1(x)\, e^{i\omega t}\right], \tag{4}$$

$$u_M(t) = \mathrm{Re}\left[u_{M1} e^{i\omega t}\right]. \tag{5}$$

We are concerned with the local enthalpy flow given by

$$\dot{H} = \int \left(\rho_m c_p \ \mathrm{Re}\left[T_1 \widetilde{u_1}\right] + (1 - T_m\beta) \ \mathrm{Re}\left[p_1 \widetilde{u_1}\right]\right) \ dA_{\mathrm{gap}} + \int \left(\rho_S c_S \ \mathrm{Re}\left[T_{S1} \widetilde{u_{S1}}\right]\right) \ dA_S, \tag{6}$$

where ρ_m, c_p, and β are the gas's mean density, specific heat, and expansion coefficient, the subscript S refers to solid properties, tilde ~ represents complex conjugation, and the integration of the gas expression is over the cross sectional area of the gap while the solid integration covers the cross sectional area of the moving one- or two-layer solid. Non-ideal-gas properties are accounted for by $T_m\beta \neq 1$, and the fact that c_p and ρ_m deviate from ideal gas values . The mean temperature gradient dT_m/dx, mean and oscillatory pressure amplitude, volume flow rate, and their x dependences are taken as known by other means such as a system model of the cooler.

The oscillatory velocity is obtained from thermoacoustic theory [4] and is

$$u_1 = \left(\frac{U_1}{A_{\mathrm{gap}}} - \frac{f_\nu u_{M1}}{2}\right) \frac{1 - h_{\nu c}}{1 - f_\nu} + \frac{u_{M1}}{2} \left(h_{\nu c} + h_{\nu s}\right), \tag{7}$$

where f_ν, $h_{\nu c}$, and $h_{\nu s}$ are among a set of functions that recur often in these calculations:

$$f_j = \frac{\tanh\left[(1+i)\, y_j/\delta_j\right]}{(1+i)\, y_j/\delta_j}, \tag{8}$$

$$g_j = \tanh\left[(1+i)\, y_j/\delta_j\right], \tag{9}$$

$$h_{jc}(y) = \frac{\cosh\left[(1+i)\, y/\delta_j\right]}{\cosh\left[(1+i)\, y_j/\delta_j\right]}, \tag{10}$$

$$h_{js}(y) = \frac{\sinh\left[(1+i)\, y/\delta_j\right]}{\sinh\left[(1+i)\, y_j/\delta_j\right]}. \tag{11}$$

When the subscript j is ν or κ, the function refers to the gas and δ_j becomes the viscous or thermal penetration depth, which are defined by $\delta_\nu^2 = 2\mu/\omega\rho_m$ or $\delta_\kappa^2 = 2k/\omega\rho_m c_p$, and $y_j = y_0$. The gas viscosity is μ and its thermal conductivity is k. When the subscript j indicates one of the solids, then δ_j is the solid thermal penetration depth of that solid, given by $\delta_S^2 = 2k_S/\omega\rho_S c_S$, and y_j is the solid's thickness L_S.

The starting point for determining the complex temperature amplitude T_1 in the gas is the generalized heat transfer equation written to first order [4]:

$$\rho_m c_p \left[i\omega T_1 + u_1 \frac{dT_m}{dx}\right] - i\omega T_m \beta p_1 = k \frac{d^2 T_1}{dy^2}. \tag{12}$$

Using equation (7) for u_1, the solution of this differential equation for T_1 is

$$T_1 = A h_{\kappa s} + B h_{\kappa c} + \frac{T_m\beta}{\rho_m c_p} p_1 - \frac{U_1}{i\omega A_{\mathrm{gap}}} \frac{dT_m}{dx} \frac{1 - \sigma + \sigma h_{\nu c}}{(1-\sigma)\,(1 - f_\nu)} + \frac{u_{M1}}{2i\omega} \frac{dT_m}{dx} \left[\frac{f_\nu}{(1-f_\nu)} + \frac{\sigma}{(1-\sigma)} h_{\nu s} + \frac{\sigma}{(1-\sigma)\,(1-f_\nu)} h_{\nu c}\right], \tag{13}$$

where the complex constants A and B must be determined by the temperature and heat-flux boundary conditions at $\pm y_0$ using properties of the solids.

The physical interpretation of equation (13) is that the gas temperature in the gap is determined by the advected heat (4th and 5th terms), heat generated by pressurization (3rd

term), and heat transfer to the walls (1st and 2nd terms). Note that for the case where the wall velocity is zero, the velocity profile responsible for the U_1 term causes the advected heat to be distributed primarily in the middle of the gap, while heat from pressurization is uniformly distributed over the gap. Thus, heat transfer coefficients should be higher for pressurization as a heat source in comparison to advection. This should be true in general regardless of geometry, and especially for regenerators. Since some regenerator codes use steady flow advected heat transfer correlations and do not distinguish between advection and pressurization as sources of heat, heat transfer should be underpredicted, such that real regenerators should outperform model predictions.

To complete the calculation, the constants *A* and *B* are determined by the boundary conditions of continuity of temperature and heat flow at the solid-gas interfaces. The general solutions in the solids are sums of h_{Sc} and h_{Ss} for each solid *S*. For a two-layer solid, continuity of temperature and heat flux is imposed at the solid-solid interface, and the boundary between solid and vacuum is treated as insulating.

Application of the boundary conditions gives the following solutions for *A* and *B*:

$$A = \frac{C_{UPI}C_{BM} - C_{UPM}C_{BI}}{C_{BI}C_{AM} + C_{BM}C_{AI}}, \tag{14}$$

$$B = -\frac{C_{UPM}C_{AI} + C_{UPI}C_{AM}}{C_{BI}C_{AM} + C_{BM}C_{AI}}, \tag{15}$$

where the constants are

$$C_{AI} = 1/g_\kappa + \eta_I, \tag{16}$$

$$C_{BI} = g_\kappa + \eta_I, \tag{17}$$

$$C_{AM} = 1/g_\kappa + \eta_M, \tag{18}$$

$$C_{BM} = g_\kappa + \eta_M, \tag{19}$$

$$\begin{aligned} C_{UPI} = {} & \eta_I \frac{T_m\beta}{\rho_m c_p} p_1 - \left(\eta_I + \sqrt{\sigma} g_\nu\right) \frac{U_1 \, dT_m/dx}{i\omega A_{\text{gap}} (1-\sigma)(1-f_\nu)} \\ & + \left[\eta_I f_\nu - (1-f_\nu)\frac{\sqrt{\sigma}}{g_\nu} + \sqrt{\sigma} g_\nu\right] \frac{u_{M1} \, dT_m/dx}{2i\omega (1-\sigma)(1-f_\nu)}, \end{aligned} \tag{20}$$

$$\begin{aligned} C_{UPM} = {} & \eta_M \frac{T_m\beta}{\rho_m c_p} p_1 - \left(\eta_M + \sqrt{\sigma} g_\nu\right) \frac{U_1 \, dT_m/dx}{i\omega A_{\text{gap}} (1-\sigma)(1-f_\nu)} \\ & + \left[\eta_M (2-f_\nu) + (1-f_\nu)\frac{\sqrt{\sigma}}{g_\nu} + \sqrt{\sigma} g_\nu\right] \frac{u_{M1} \, dT_m/dx}{2i\omega (1-\sigma)(1-f_\nu)}. \end{aligned} \tag{21}$$

The different forms of the boundary conditions in the solids themselves give different forms of the constants η_I and η_M which account for the immobile and moving solids' thermal influences on the gas. For a single-layer solid that is insulated on the outside,

$$\eta_S = \frac{k_S \delta_\kappa}{k \delta_S} g_S = \sqrt{\frac{k_S \rho_S c_S}{k \rho_m c_p}} \tanh\left[(1+i) L_S/\delta_S\right]. \tag{22}$$

For a two-layer wall, also insulated on the outside,

$$\eta_{2\text{layer}} = \eta_a \frac{1 + \eta_b/\eta_a}{1 + g_a^2 \eta_b/\eta_a}, \tag{23}$$

where the subscript *a* refers to the layer adjacent to the gas and *b* refers to the layer farther from the gas.

The temperature of a single-layer immobile solid can then be obtained from

$$T_{I1} = T_1(\pm y_0)\ h_{Ic}, \tag{24}$$

where $+y_0$ or $-y_0$ is chosen depending on which side of the gap the solid is on. The zero of the argument of the function h_{Ic} is on its insulated side, as shown in FIGURE 1. Similarly, the temperatures in a two-layer immobile solid are

$$T_{Ia1} = \frac{T_1(\pm y_0)}{1 + g_a^2 \eta_b/\eta_a} \left(h_{ac} + \frac{g_a^2 \eta_b}{\eta_a} h_{as} \right), \tag{25}$$

$$T_{Ib1} = \frac{T_1(\pm y_0)}{(1 + g_a^2 \eta_b/\eta_a) \cosh[(1+i) L_a/\delta_a]} h_{bc}. \tag{26}$$

A single-layer moving solid is described by

$$T_{M1} = \left[T_1(y_0) + \frac{u_{M1}}{i\omega} \frac{dT_m}{dx} \right] h_{Mc} - \frac{u_{M1}}{i\omega} \frac{dT_m}{dx}, \tag{27}$$

and a two-layer moving solid is described by

$$T_{Ma1} = \frac{T_1(y_0) + (u_{M1}/i\omega)\, dT_m/dx}{1 + g_a^2 \eta_b/\eta_a} \left(h_{ac} + \frac{g_a^2 \eta_b}{\eta_a} h_{as} \right) - \frac{u_{M1}}{i\omega} \frac{dT_m}{dx}, \tag{28}$$

$$T_{Mb1} = \frac{T_1(y_0) + (u_{M1}/i\omega)\, dT_m/dx}{(1 + g_a^2 \eta_b/\eta_a) \cosh[(1+i) L_a/\delta_a]} h_{bc} - \frac{u_{M1}}{i\omega} \frac{dT_m}{dx}. \tag{29}$$

Once the temperature solution is generated, the enthalpy is calculated by integration of equation (6) over the cross-sectional areas of the gap and moving solid. For simple situations, the integrals can be done analytically without too much difficulty, but the results below were generated by performing this integration numerically.

RESULTS

The model was exercised over a range of parameters typical of a small low temperature cooler. Representative results are plotted below to illustrate some of the observed behavior. FIGURE 2 shows T_1 at a particular point during a cycle plotted as a function of position for the solid region of one wall, the gas region, and the second solid region consisting of a layered wall. At the temperature of 40 K, the real part has a temperature amplitude of 0.6 K. The wall heat capacity is not sufficiently high enough to keep the gas temperature oscillations at zero at the boundaries, and the differing wall heat capacities pin the gas temperatures at different values at the two walls. The wall velocity is zero for this example.

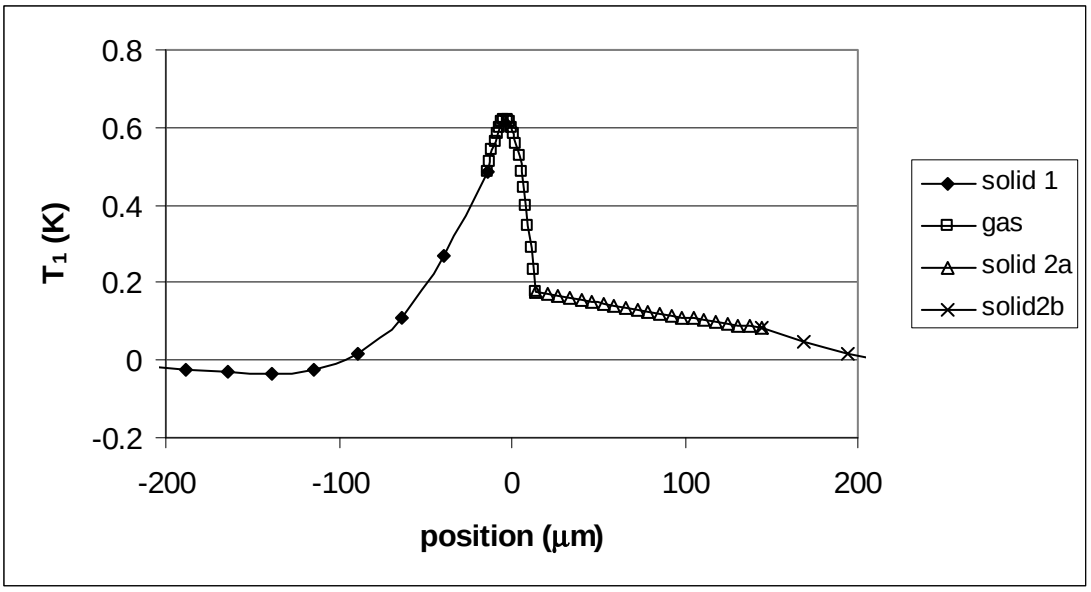

FIGURE 2. Temperature solution at 40 K at a particular time during a cycle. Wall velocity is zero, and the solid boundaries extend well beyond the scale on this plot.

FIGURE 3 shows a solution for the same flow and pressures used to generate FIGURE 2, but at 15 K. Here, the temperature amplitude is significantly higher at around 1.5 K, which results in substantially higher enthalpy flow. Both the temperatures at the walls, plus the temperature difference between the gas in the middle of the gap and the walls, are larger than at 40 K.

FIGURE 4 illustrates the detrimental effects of diminishing solid heat capacity, increasing gas heat capacity, and decreasing gas penetration depth. The enthalpy flow in the gas, the shuttle loss, and the total combined loss corresponding to different temperature points along a displacer gap is shown for one particular design. This plot shows

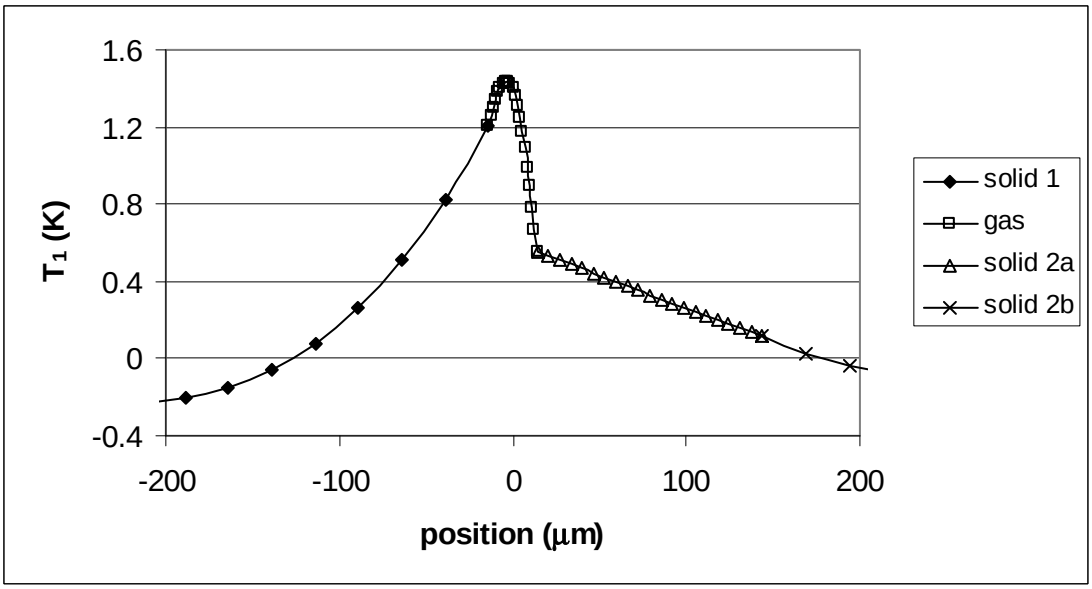

FIGURE 3. Temperature solution at 15 K using flow and pressures from the system model used in FIGURE 2.

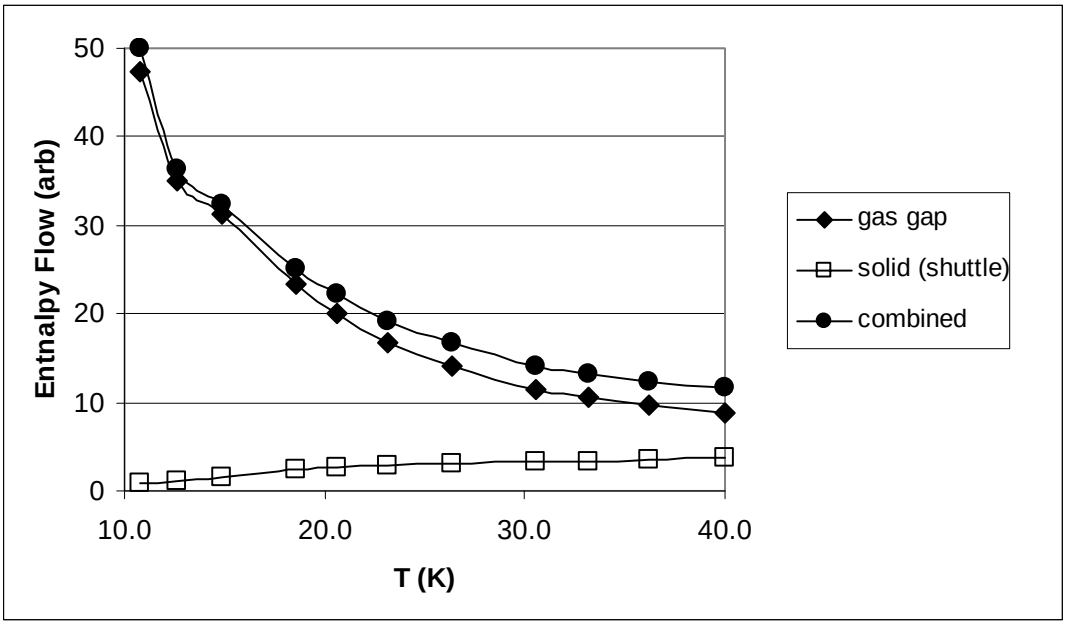

FIGURE 4. Enthalpy flow as a function of temperature showing a significant increase in gap loss as the temperature decreases.

that for the colder sections of the gap, the total loss increases dramatically and is substantial. Below 20 K, the shuttle term decreases as expected but is overwhelmed by the enthalpy flow in the gas gap. This plot was generated assuming a constant temperature gradient. For a real gap, thermal isolation forces the enthalpy flow to be constant, such that the temperature gradient will adjust accordingly and the actual enthalpy flow will be some weighted average of that shown in FIGURE 4. This result is sensitive to details of the gap and flows, so an optimized design can reduce these losses. The results in the plot also indicate that the total loss is nearly equal to the sum of the two individual losses. In other cases, however, coupling between the loss mechanisms can produce a total loss that may not equal the sum of the two losses.

Real gas effects, to first order, appear as deviations of $T_m\beta$, $\rho_m c_p$, thermal conductivity and viscosity from ideal gas values. In the temperature region shown in FIGURE 4, real gas effects in $\rho_m c_p$ increases the enthalpy at 10K by around 30%, and effects from non-ideal gas behavior of $T_m\beta$ and the transport properties are less than 10% effects. The fact that $\rho_m c_p$ increases at low temperature, regardless of real gas effects, is the largest contributor to the enthalpy increase. Pressure dependence of $\rho_m c_p$ and $T_m\beta$ require a substantially more involved 4^{th} order calculation and is beyond the scope of this work.

CONCLUSIONS

A thermoacoustic analysis for a displacer gap at low temperatures has been developed, which includes the effects of thermal penetration depth being comparable to the width of the gap, and finite but differing heat capacities on the adjoining solid walls, which can have one or two layers. Results of a typical Stirling design indicate that enthalpy loss can significantly increase at low temperatures, partly due to diminishing wall heat capacity, and partly due to reduced thermal penetration depths in the gas. Since these results are design specific, they must be applied on a case-by-case basis.

ACKNOWLEDGMENT

One of us (GS) gratefully acknowledges the support of the US DOE's Office of Basic Energy Sciences.

REFERENCES

1. Ward, W. C., and Swift, G. W., "Design Environment for Low Amplitude Thermoacoustic Engines," *J. Acoust. Soc. Am.* **95**, 3671-3672 (1994); www.lanl.gov/thermoacoustics.
2. Gedeon, D., *Sage Stirling-Cycle Model Class Reference Guide,* Third Edition, Gedeon Associates, Athens, OH (1999)
3. Gary, J., and Radebaugh, R., "An Improved Numerical Model for Calculation of Regenerator Performance (REGEN3.1)," in *Proc. of the Fourth International Meeting on Cryocoolers,* No. DTRC-91/003, David Taylor Research Center, Bethesda, MD, 1991, pp 165-176
4. Swift, G. W., *Thermoacoustics: A Unifying Perspective for Some Engines and Refrigerators,* Acoustical Society of America Publications, Sewickley PA, 2002.